Supplementary Information (SI) for ChemComm.

Supplementary information

Designing interfacially stable Na-ion polymer electrolytes with tailored local solvation structures

Jun Pan[a#], Xinran Gao[b#], Yanhong Liu[c], Okkyun Seo[d], Rosantha Kumara[d], Yuwei Liu[d], Takeshi Watanabe[d], Bing Zhu[a], Zhongchao Bai[b], Shixue Dou[b], Nana Wang[e*], Dongshuang Wu[a*]

[a] School of Materials Science & Engineering, Nanyang Technological University, Singapore 639798, Singapore

[b] Institute of Energy Materials Science, University of Shanghai for Science and Technology, Shanghai 200050, P. R. China

[c] School of Radiology, Shandong First Medical University & Shandong Academy of Medical Sciences, Taian 271000, China

[d] Center for Synchrotron Radiation Research, Japan Synchrotron Radiation Research Institute (JASRI), 1-1-1 Kouto, Sayo, Hyogo 679-5198, Japan

[e] Centre for Clean Energy Technology, School of Mathematical and Physical Sciences, Faculty of Science, University of Technology Sydney, Sydney, New South Wales 2007, Australia

[#]Jun Pan and Xinran Gao contributed equally to this work.

*Corresponding author.

Experimental Section

All the chemicals were bought and directly used without any further purification.

Preparation of gel polymer electrolytes (GPEs): To prepare GPEs, polyvinylidene fluoride-hexafluoropropylene (P(VDF-HFP), 1.0 g, Aladdin, average Mw ~400,000), sodium bis(trifluoromethylsulfonyl)imide (NaTFSI, 0.45 g, Alfa Aesar), azodicarbonamide (ADA, 0.023 g, Aladdin), and propylene carbonate (PC, 1 mL, Sinopharm) were dissolved in acetone (10 mL, Sinopharm) under continuous stirring for 3 h at 55°C, followed by an additional 8 hours at room temperature. The electrolyte slurry was coated using a film scraper to a thickness of 1.0 mm and subsequently dried at 60°C, yielding a GPE with a thickness of approximately 100 μm. Control samples were prepared following the same procedure, excluding the addition of ADA.

Electrochemical measurement: The cathode was fabricated by mixing $NaFe_{1/3}Mn_{1/3}Ni_{1/3}O_2$ (NFMNO) powder, super P, and polyvinylidene fluoride in a weight ratio of 8:1:1 with 1-methyl-2-pyrrolidone as the solvent. The resulting slurry was ground for half an hour using the vacuum planetary centrifugal mixer, spread on the Al current collector, and vacuum dried at 80°C for 12 h. The dried film was then rolled and cut into disks with a diameter of 12 mm. Na metal (commercially purchased with a diameter of 14 mm) was used as the counter electrode and GPEs as the electrolytes. The cathode electrode is a small circular disc with a diameter of 12 mm, with an active material mass loading of 3-5 mg cm^{-2}. CR2032-type coin cells were assembled in an argon-filled glove box (MIKROUNA, $H_2O < 1$ ppm; $O_2 < 1$ ppm). Galvanostatic discharge/charge testing was conducted at 25°C within a voltage range of 2-4 V using a Neware battery tester (China). cyclic voltammetry (CV) and electrochemical impedance spectra (EIS) spectra (100 kHz to 0.01 Hz) measurements were performed using an electrochemical workstation (CHI760E, China) at room temperature. The Na^+ conductivity of the GPEs was evaluated using a symmetric SS|GPEs|SS (SS = stainless steel) at 25°C. Linear sweep voltammetry was conducted using Na|GPEs|SS coin cells at 25°C. Symmetrical cells were tested by sandwiching the GPE/AGPE between two identical sodium disks.

Characterization: Powder X-ray powder diffraction patterns were obtained using an X-ray diffractometer (Bruker D8 Advanced, Germany), taking monochromatic Cu Kα as a radiation source. The scanning electron microscopy (SEM) images, energy-dispersive X-ray spectra, and elemental mapping were performed on a field-emission scanning electron microscope (JEOL JSM-7600F, Japan). The transmission electron microscopy (TEM) and high-resolution TEM (HRTEM) images were taken from an aberration-corrected transmission electron microscope (JEOL F200, Japan). X-ray photoelectron spectroscopy (XPS) spectra were acquired on an X-ray Photo-electron spectrometer (AXIS SUPRA, Japan). Inductively coupled plasma atomic emission spectroscopy (ICP-AES) characterization was conducted using an emission spectrometer (PE-8000, USA). Thermogravimetric analysis (TGA) was performed using a thermal analyzer (Mettler Toledo TGA/SDTA85, Canada) from room temperature to 800 °C under an N_2 atmosphere. Fourier transform infrared (FTIR) spectra were measured using an infrared spectrum analyzer (Bruker Tensor 27). Raman spectra were acquired with a Horiba LabRAM HR spectrometer. Synchrotron-based XAS measurement was performed in transmission mode on beamline BL14b2 in Japan. The acquired X-ray absorption spectroscopy (XAS) spectra were energy-calibrated and normalized through the ATHENA software package.[1] All cell disassembly for ex-situ testing was performed in a glove box and transferred under an Ar atmosphere.

Computational methods: All Density functional theory (DFT) calculations were performed using the Gaussian 16 program.[2] Geometries optimizations of stationary points were conducted with the M06 functional[3] employing the 6-311+G(d,p)[4] for all atoms. Frequency analyses were calculated at the same level of theory to confirm the optimized structures to be local minima (with zero imaginary frequency). The Gibbs free energy changes were calculated using the following equation:

$$\Delta G^{\mathrm{r}} = G(\mathrm{pro}) - G^{1}(\mathrm{react}) - G^{2}(\mathrm{react})$$

where the ΔG^{r}, $G(\mathrm{pro})$, $G^{1}(\mathrm{react})$, and $G^{2}(\mathrm{react})$ are the Gibbs free energies of reaction energy, product, reactant 1, and reactant 2, respectively.

Supplementary Figures

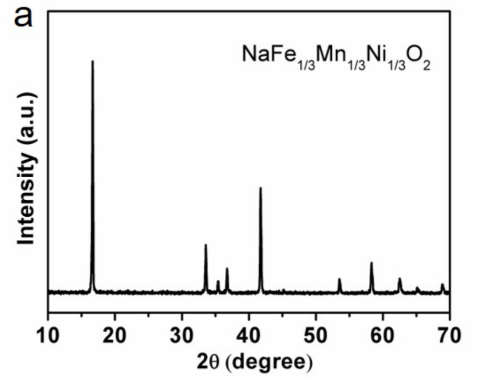

b

Element	Weight%	Atomic%
O	32.75	54.31
Na	20.6	23.17
Mn	15.84	7.65
Fe	14.65	6.96
Ni	16.16	7.3
Totals	100	100

Fig. S1. Composition characterization of NFMNO. (a) XRD pattern. (b) EDS spectrum.

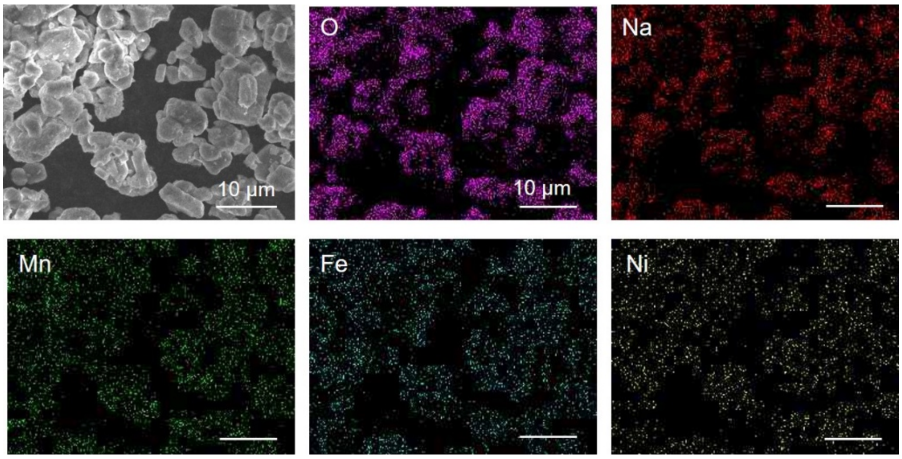

Fig. S2. SEM image and the corresponding elemental mapping of the NFMNO.

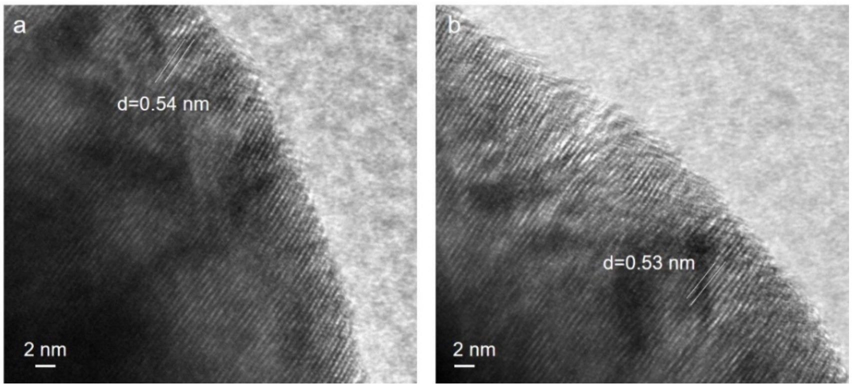

Fig. S3. (a,b) Two representative HRTEM images of the NFMNO.

The commercially purchased NFMNO cathode exhibits a hexagonal crystal structure (space group: R-3m, No. 166) (Fig. S1).[5] The particle size ranges from 2 to 5 μm, with a uniform distribution of elements throughout (Fig. S2). High-resolution transmission electron microscopy (HRTEM) images show that the interlayer spacing of NFMNO is about 0.54 nm (Fig. S3), which is consistent with the X-ray diffraction pattern.[6]

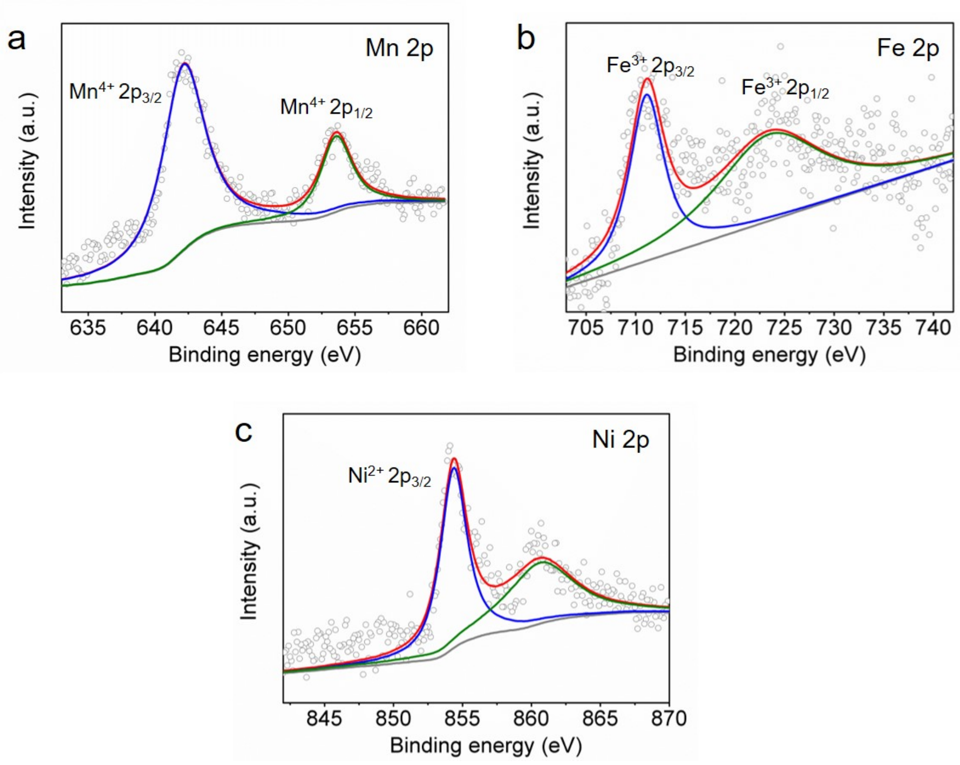

Fig. S4. XPS spectra of the NFMNO. (a) Mn 2p, (b) Fe 2p, (c) Ni 2p.

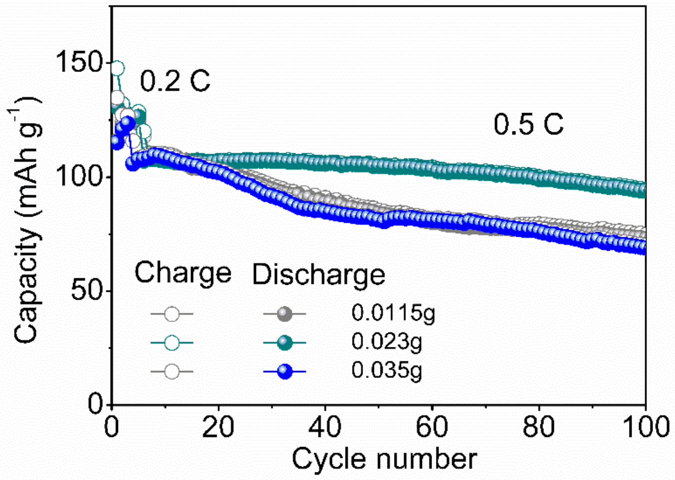

Fig. S5. Cycling performances of the NFMNO//GPE//Na cell with different amounts of ADA additive.

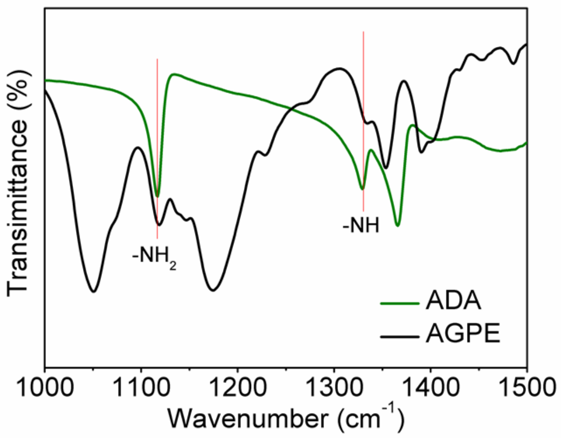

Fig. S6. FTIR spectrums of ADA and AGPE.

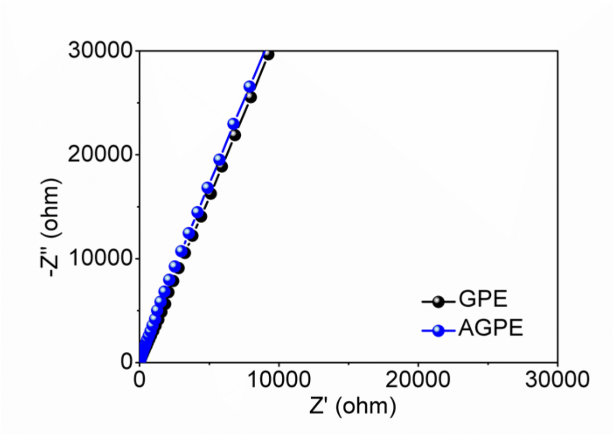

Fig. S7. EIS spectra of the prepared GPE and the AGPE films.

According to the formula $\sigma = l/R*S$, $\sigma_{GPE} = 0.00114\ cm/3.789\ \Omega \times 3.14 \times (0.75\ cm)^2 = 1.7 \times 10^{-3}$ S/cm and $\sigma_{AGPE} = 0.00217\ cm/3.716\ \Omega \times 3.14 \times (0.75\ cm)^2 = 3.3 \times 10^{-3}$ S/cm are obtained (Fig. 2d).

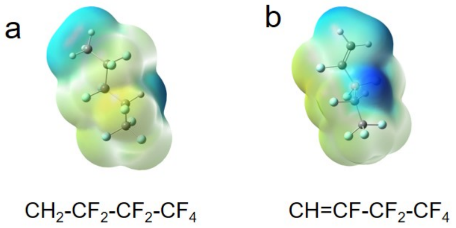

Fig. S8. Electrostatic potential of (a) CH_2-CF_2-CF_2-CF_4, and (b) CH=CF-CF_2-CF_4 structures.

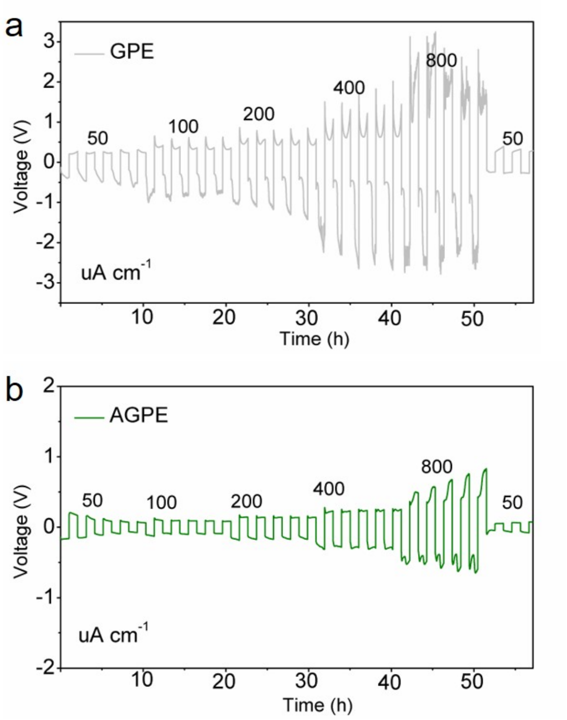

Fig. S9. Cycling performance of (a) Na//GPE//Na and (b) Na//AGPE//Na symmetric cells with different current densities at 25 °C.

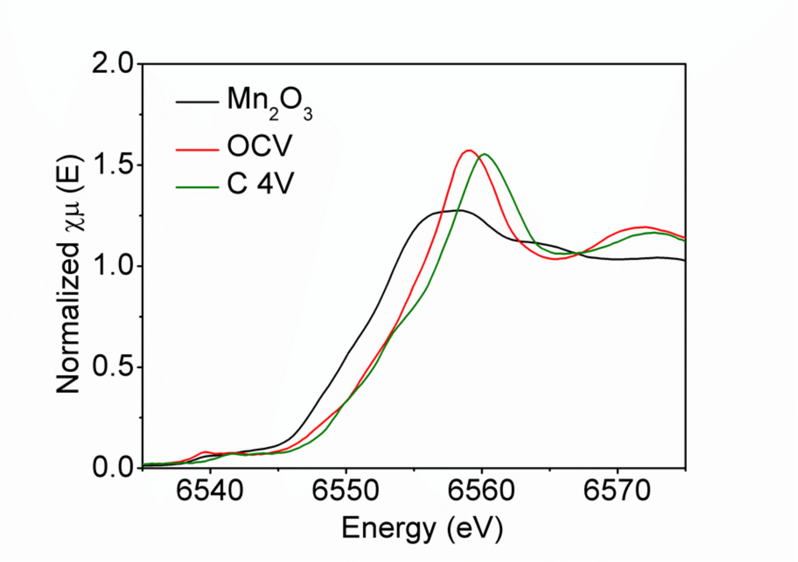

Fig. S10. Normalized X-ray absorption near edge structure (XANES) spectra of Mn K-edges at different states in NFMNO//GPE//Na cell. Mn_2O_3 powder is the reference sample.

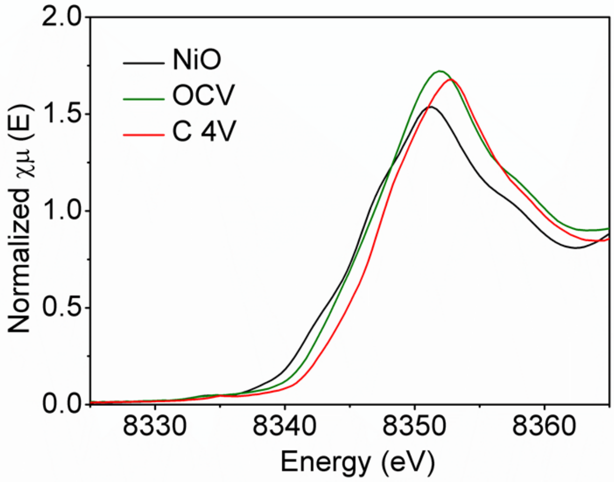

Fig. S11. Normalized XANES spectra of Ni K-edges at different states in NFMNO//GPE//Na cell. NiO powder is the reference sample.

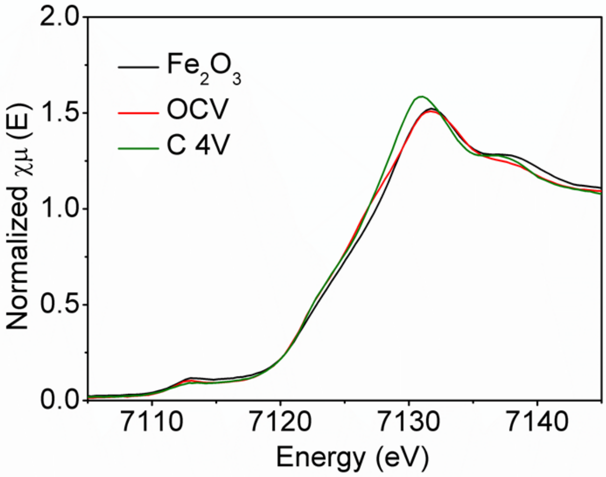

Fig. S12. Normalized XANES spectra of Fe K-edges at different states in NFMNO//GPE//Na cell. Fe_2O_3 is the reference sample.

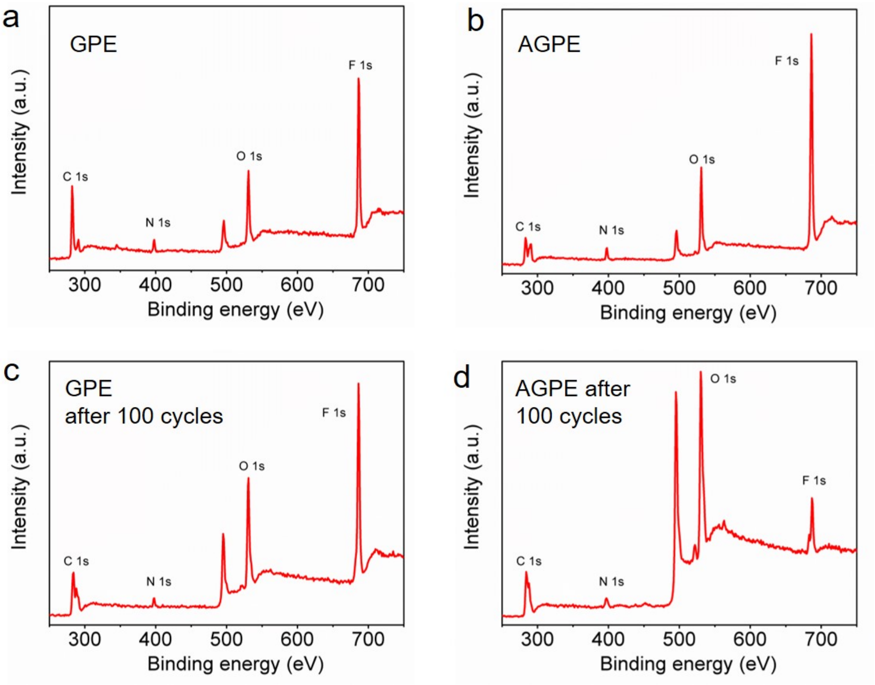

Fig. S13. XPS survey spectra. (a) Uncycled GPE. (b) Uncycled AGPE. (c) GPE in the NFMNO//Na cell after 100 cycles. (d) AGPE in the NFMNO//Na cell after 100 cycles.

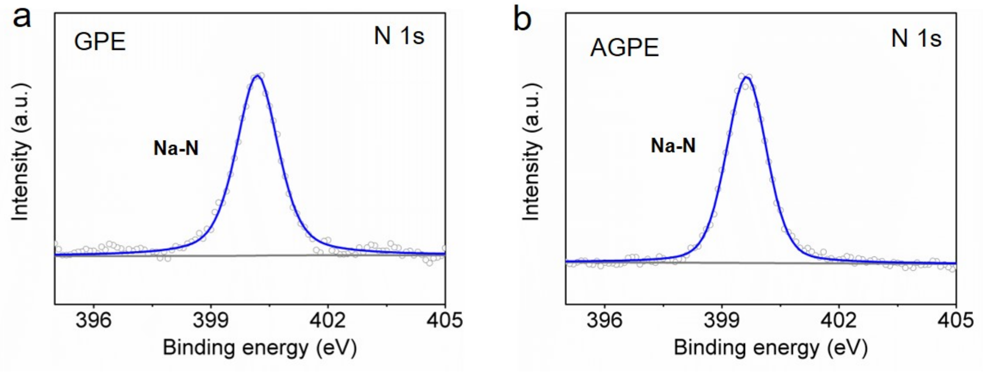

Fig. S14. XPS spectra of N 1s. (a) Uncycled GPE. (b) Uncycled AGPE.

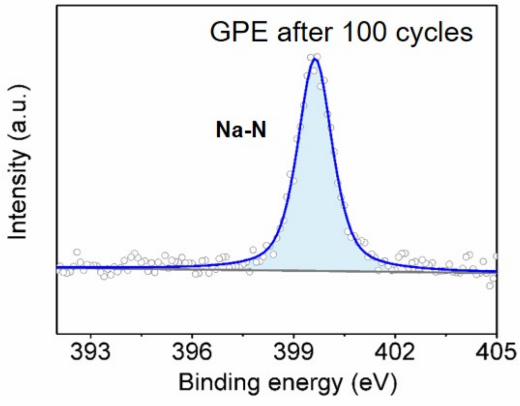

Fig. S15. XPS spectra of the polymer electrolytes (N 1s) after 100 cycles.

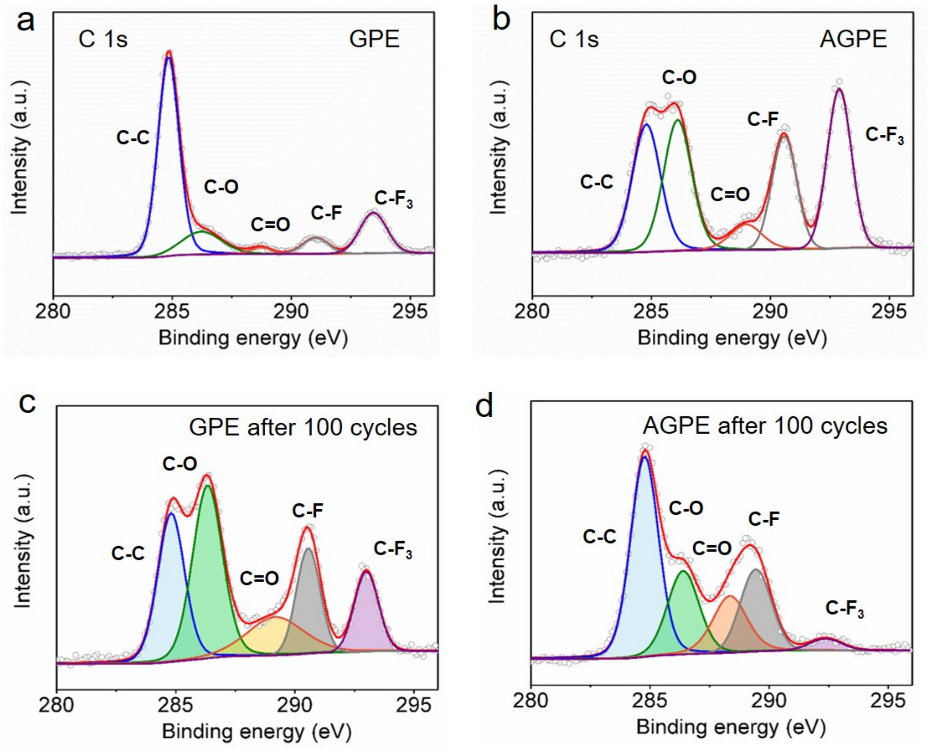

Fig. S16. XPS spectra of C 1s. (a) Uncycled GPE. (b) Uncycled AGPE. (c,d) XPS spectra of the polymer electrolytes (C 1s) after 100 cycles.

As shown in the C 1s spectra (Fig. S16), the content of C=O in GPE before cycling is less than that of AGPE. This may be explained that during the vacuum process, the PC solvent is removed, resulting in less residual PC in GPE, whereas AGPE retains more PC due to bonding.

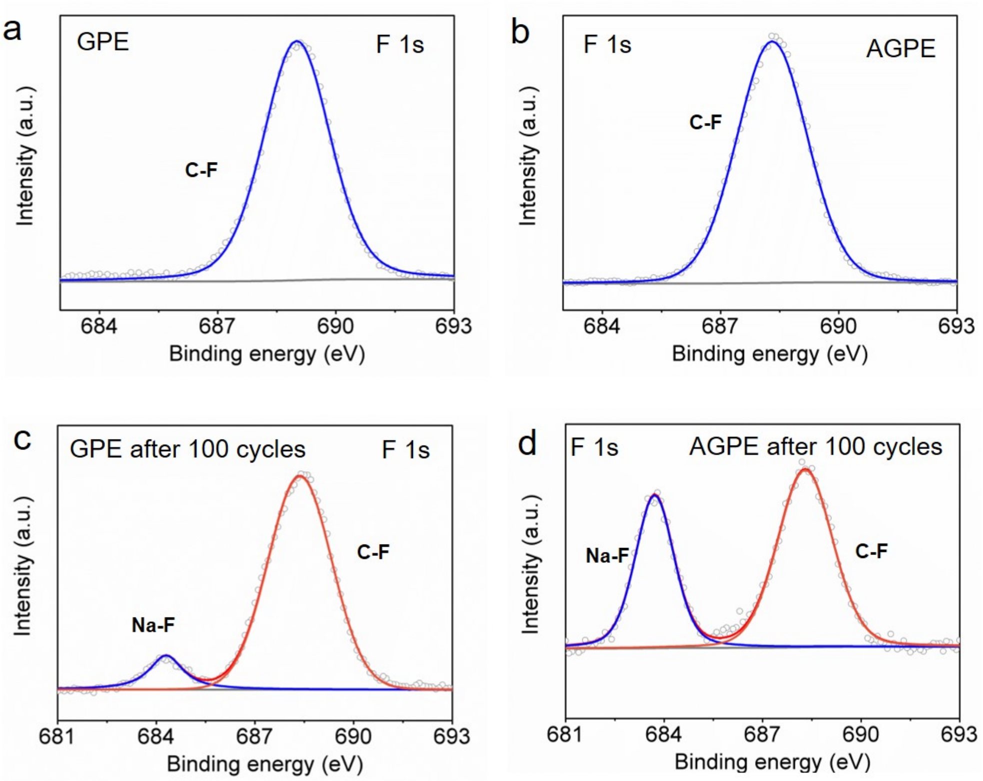

Fig. S17. XPS spectra of F 1s. (a) Uncycled GPE. (b) Uncycled AGPE. (c) GPE in the NFMNO//Na cell after 100 cycles. (d) AGPE in the NFMNO//Na cell after 100 cycles.

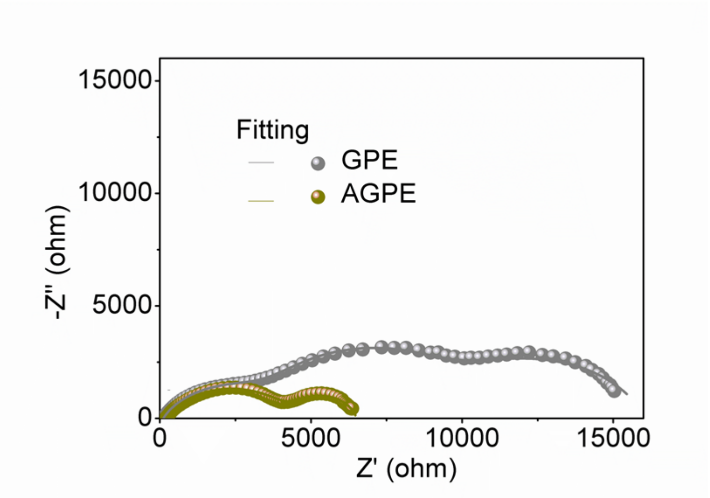

Fig. S18. EIS spectra and the fitting curves of the NFMNO//GPE//Na cell and the NFMNO//AGPE//Na cell after 50 cycles.

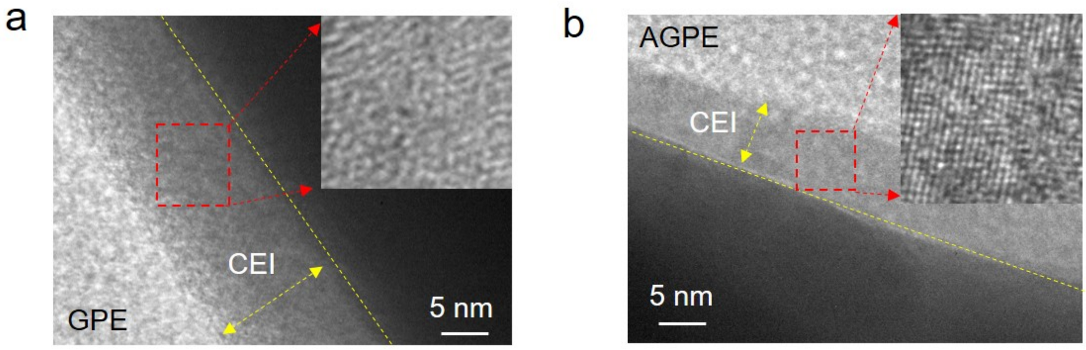

Fig. S19. (a,b) HRTEM images of the cathode interface.

Transmission electron microscopy (TEM) characterization reveals that the CEI film of the NFMNO in the NFMNO//AGPE//Na cell is about 8 nm thick, slightly thinner than that in the NFMNO//GPE//Na cell (12 nm) (Figs. 4b and 4c). Upon magnification, the lattice fringes of the CEI film indicate a higher concentration of inorganic substances containing additives for the AGPE-based cell. This structural composition enhances the conduction of sodium ions and aligns with the results obtained from EIS.

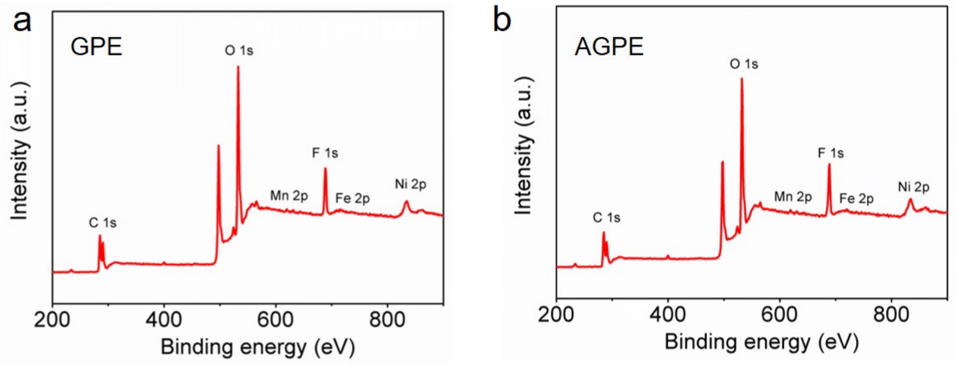

Fig. S20. XPS survey. (a) NFMNO in the NFMNO//GPE//Na cell after 3 cycles. (b) NFMNO in the NFMNO//GPE//Na cell after 3 cycles.

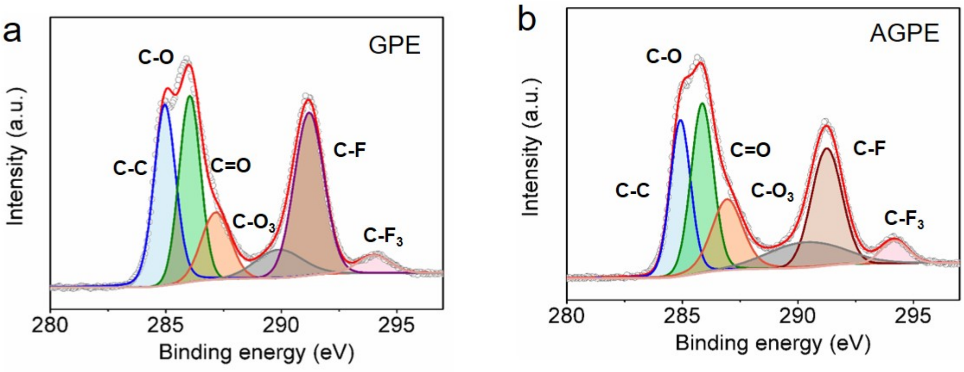

Fig. S21. (a,b) XPS spectra of the cathode surface (C 1s) after 3 cycles.

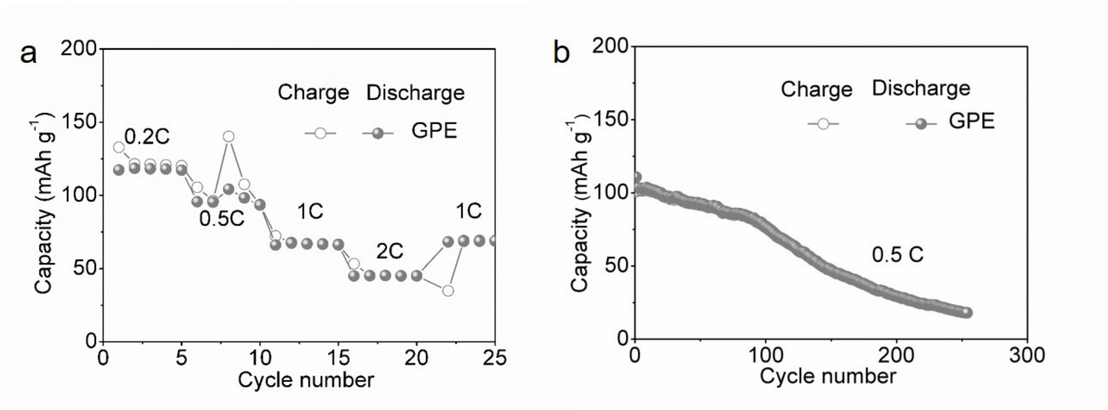

Fig. S22. (a,b) Rate performances and cycling performance of the NFMNO//GPE//Na cell.

Supplementary Tables

Table S1. Reaction heat calculated by DFT.

	G (Hartree)	ΔG (kcal/mol)
PC	-381.5396	
CH2-CF2-CF2-CF4	-991.5378	
CH=CF-CF2=CF4	-891.0632	
PC…CH2-CF2	-1373.065	7.6186
PC…CH=CF	-1272.5959	4.3562

Table S2. Fitting results for EIS spectra after 3 cycles.

After 3 cycles	R_s (Ω)	R_f (Ω)	R_{ct} (Ω)
GPE	52.1	4080	5162
AGPE	55.8	1425	5893

Table S3. Fitting results for EIS spectra after 50 cycles.

After 50 cycles	R_s (Ω)	R_f (Ω)	R_{ct} (Ω)
GPE	119.1	10393	5537
AGPE	212.4	2109	4186

References

1. B. Ravel and M. Newville, *J. Synchrotron Radiat.*, 2005, **12**, 537-541.

2. M. J. Frisch, G. W. Trucks, H. B. Schlegel, G. E. Scuseria, M. A. Robb, J. R. Cheeseman, G. Scalmani, V. Barone, G. A. Petersson, H. Nakatsuji, X. Li, M. Caricato, A. V. Marenich, J. Bloino, B. G. Janesko, R. Gomperts, B. Mennucci, H. P. Hratchian, J. V. Ortiz, A. F. Izmaylov, J. L. Sonnenberg, D. Williams-Young, F. Ding, F. Lipparini, F. Egidi, J. Goings, B. Peng, A. Petrone, T. Henderson, D. Ranasinghe, V. G. Zakrzewski, J. Gao, N. Rega, G. Zheng, W. Liang, M. Hada, M. Ehara, K. Toyota, R. Fukuda, J. Hasegawa, M. Ishida, T. Nakajima, Y. Honda, O. Kitao, H. Nakai, T. Vreven, K. Throssell, J. A. Montgomery, J. E. J. Peralta, F. Ogliaro, M. J. Bearpark, J. J. Heyd, E. N. Brothers, K. N. Kudin, V. N. Staroverov, T. A. Keith, R. Kobayashi, J. Normand, K. Raghavachari, A. P. Rendell, J. C. Burant, S. S. Iyengar, J. Tomasi, M. Cossi, J. M. Millam, M. Klene, C. Adamo, R. Cammi, J. W. Ochterski, R. L. Martin, K. Morokuma, O. Farkas, J. B. Foresman, D. J. Fox, Gaussian 16, Revision A.03; Gaussian, Inc.: Wallingford, CT, 2016.

3. Y. Zhao and D. G. Truhlar, *Theor. Chem. Acc.*, 2008, **120**, 215-241.

4. S. Huzinaga, *Comput. Phys. Rep.*, 1985, **2**, 281-339.

5. H. Wang, X. Z. Liao, Y. Yang, X. M. Yan, Y. S. He and Z. F. Ma, *J. Electrochem. Soc.*, 2016, **163**, A565-A570.

6. Y. Y. Xie, H. Wang, G. L. Xu, J. J. Wang, H. P. Sheng, Z. H. Chen, Y. Ren, C. J. Sun, J. G. Wen, J. Wang, D. J. Miller, J. Lu, K. Amine and Z. F. Ma, *Adv. Energy Mater.*, 2016, **6**, 1601306.